



## A Two-scale Topology Optimization Method for Functionally Graded Lattice Structures using Three Families of Micro-Structures

Ahmed Mohamed Jubartalla Ali<sup>1,2</sup> , Lisa-Marie Faller<sup>1,\*</sup> , Margit Gföhler<sup>2</sup> , Franz Oswald Riemelmoser<sup>1</sup> , Mario Kapl<sup>1</sup> 

<sup>1</sup>ADMIRE Research Center, Carinthia University of Applied Sciences,  
[a.ali, f.riemelmoser, m.kapl}@fh-kaernten.at](mailto:{a.ali, f.riemelmoser, m.kapl}@fh-kaernten.at)

<sup>2</sup>Faculty of Mechanical and Industrial Engineering, TU Wien, [margit.gfoehler@tuwien.ac.at](mailto:margit.gfoehler@tuwien.ac.at)

\*The author was affiliated with 1 at the time of this study and is currently an independent scholar,  
[lisamariefaller8@gmail.com](mailto:lisamariefaller8@gmail.com)

Corresponding author: Ahmed Mohamed Jubartalla Ali, [a.ali@fh-kaernten.at](mailto:a.ali@fh-kaernten.at)

**Abstract.** Firstly, a novel unit cell design, denoted as XX-shaped and constructed by horizontally stacking two X-shaped structures, is introduced. The new design shows lower compliance and telling mechanical properties compared to the original X-shaped structure. Secondly, three series of micro-structures that share similar geometric features are constructed and grouped into three families: The first is conventional and widely used in the literature and contains superimposed parameterized X-shaped and square-shaped lattices. The second is new and consists of superimposed parameterized XX-shaped and square-shaped lattices while the third is generated by rotating the components of the second family by 90°. Thirdly, a novel two-scale topology optimization procedure to build macro-structures from the predefined micro-structures of the three families is presented. In order to overcome the obstacle of finding suitable initial guesses for the design variables, the optimization process of material (macro-scale) and lattice (micro-scale) distributions is conducted in three steps. In each step, a distinct set of design variables is optimized. The modified Porous Anisotropic Material with Penalization is used to model the micro-structures and their effective properties are obtained by the numerical homogenization method. Finally, representative 2D numerical structural compliance minimization problems are solved to illustrate the potential and effectiveness of the new designs, where the results show that using hybrid lattice structures from the three families together can achieve better structural performance than just employing the conventional family.

**Keywords:** Multi-scale structures, parameterized lattice, multiple design variables, homogenization

**DOI:** <https://doi.org/10.14733/cadaps.2024.179-198>

## 1 INTRODUCTION

Michell's paper on the optimal design of frame structures [20] can be seen as a seminal work in the field of topology optimization (TO). He showed how to find the lightest possible frame structure that could support a given set of loads and constraints. Recent developments in topology optimization have extended Michell's work by incorporating advanced computational tools such as the finite element method (FEM) and two-scale structure concepts. These methods allow for the optimization of complex, functionally graded lattice structures, which can offer superior mechanical performance compared to traditional designs.

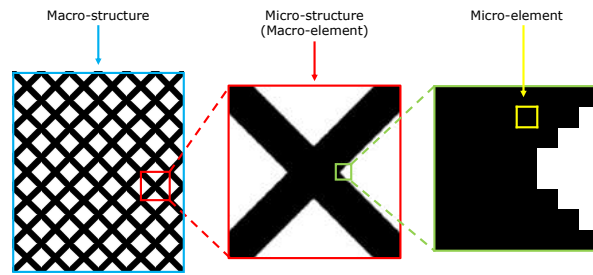
A common TO objective is minimizing compliance, in which algorithms increase structures' stiffness by redistributing the material within the specified design domain. An important approach presented by [22] uses TO to simultaneously optimize the shape and material distribution of the compliant mechanism in order to achieve a desired output behavior. This method has been shown to be highly effective in producing complex, high-performance compliant mechanisms that are difficult or impossible to design using traditional methods. This is accomplished by firstly, discretizing the structure into  $N$  finite elements and assigning a relative density value  $\rho_n$  to each element  $n$ . Then, a relation between the densities and compliance is established through the modulus. After that, the set of densities,  $\rho = \{\rho_1, \rho_2, \dots, \rho_N\}^T$ , is considered as a variable of an optimization problem and the optimized values are used to represent the topology of the optimized structure.

Due to the freedom in design and light-weighting possibilities offered by Additive Manufacturing (AM), TO has attracted the attention of researchers in many fields such as medical implants, aerospace, as well as mechanical and civil engineering [1, 19, 35]. Cellular structures are widely used in lightweight design due to their high strength-to-weight ratio. In addition, the structural performance of AM cellular structures can be easily modified by changing their design parameters, e.g. the strut diameter, according to the structural requirement. These structures are known as Functionally Graded Lattice structures (FGLs).

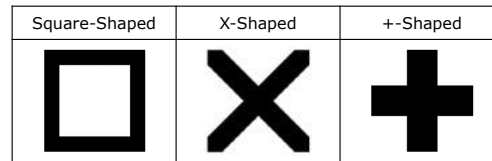
Optimizing cellular structures requires very fine meshes. To alleviate the related high computational cost of a very fine mesh representation in FEM, it is very practical to employ the approach of multi-scale modeling, in which the design domain of the macro-scale structure (or simply macro-structure) is firstly discretized into a sufficient number of subdomains called macro-elements, micro-scale structures, or simply micro-structures. Then, these micro-structures are discretized into fine elements called micro-scale elements or simply micro-elements. To ensure that continuum mechanics applies to both the macro- and micro-scale structures, the micro-elements need to be much smaller than the macro-elements, which is known as the separation of length scales. A typical two-scale structure is shown in Fig. 1a.

A common method to solve multi-scale TO problems is to assemble the design variables of each scale in a separate set and then optimize these sets simultaneously. This concurrent approach was used in many recent designs including two-variable optimization [5, 18, 21, 24, 33], three-variable optimization [4, 6, 7], and four or more design variables optimization [8, 12, 13, 31]. Generally, when optimizing multi-scale structures, a homogenization method is used to evaluate the effective material properties of the micro-structures by solving specific partial differential equations either analytically (for simple micro-structures) or numerically (for complicated micro-structures) by using the FEM which is computationally expensive [10, 11].

To pursue time reduction during the optimization of FGLs, the optimization process can be restricted to a group of predefined lattices, which consequently restricts the application of the numerical homogenization to a limited number of cycles. A better alternative to the groups of predefined lattices is using a family consisting of micro-structures having similar geometric features. In literature, many works addressing two-scale TO algorithms rely on one common family of micro-structures. This conventional family is generated by superimposing two parameterized common micro-structures; the square-shaped (equivalent to the  $+$ -shaped) and X-shaped because of their superior in-plane mechanical properties. Additional intermediate lattices are constructed by varying the value of the design variable  $\varphi$ , for instance,  $\varphi = 0$  indicates the square-shaped micro-structure,  $\varphi = 1$  indicates the X-shaped micro-structure, and  $0 < \varphi < 1$  indicates a linear combination between them considering that the volume is constant for all these lattices. Fig. 1b illustrates the square-shaped,  $+$ -



(a) Two-scale structure



(b) Selected micro-structures.

$$\text{family} = \left\{ \varphi \left( \text{X} \right) \cup (1 - \varphi) \left( \text{Square} \right), \quad \text{for } 0 \leq \varphi \leq 1 \right\}$$

Parameter $\varphi$	0	...	0.294	...	0.647	...	1
Micro-structure		...		...		...	

(c) Family of micro-structures

**Figure 1:** (a) Two-scale structure, (b) selected micro-structures, and (c) a family of micro-structures.

shaped, and X-shaped lattices and Fig. 1c shows a family of parameterized micro-structures occupying 50 % of its design domain, i.e., having a micro-scale volume fraction of  $V_f^{\text{MI}} = 50\%$ , which has been used in the seminal formulation of Wang et al [25]. Then, extensions accounting for variable micro-scale volume fractions were successfully introduced in [16, 26], but they were limited to the same family of micro-structures. After that, non-symmetric micro-structures but also from the conventional family were added. Their micro-scale volume fractions were fixed in [15, 27, 30] and then allowed to vary in [32, 34].

In this work, we present two additional families of micro-structures together with a two-scale topology optimization procedure to enhance the structural performance of the optimized FGLs. The consideration of the three families is important from both an implementation point of view and an engineering point of view. In the former, numerical stability difficulties such as alternating between the families and local minima while the gain, achieved in the latter, is increased flexibility. Our proposed procedure accounts for three design variables wherein two of which are used to navigate between and within the three families. The optimization process is done in three steps. In each step, and as a strategy to reduce the initial guess dependency, only a subset of the design variables is optimized. However, we start by optimizing only the element densities (first

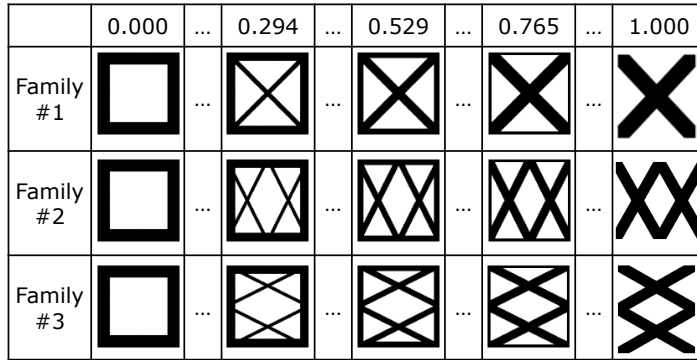


**Figure 2:** Selected micro-structures members from the three families.

design variable) in the first step and continue optimizing them through the second and third steps. In the second step, the families are selected by optimizing the second design variable, whereas the micro-structures are selected by optimizing the third design variable in the third step. The remainder of this manuscript is organized as follows: In Sec. 2, the design of the newly proposed families is discussed besides a brief introduction of the numerical homogenization. In addition, the design of the macro-structure is described. In Sec. 3, the formulation and solution of the TO problem include the definition of the design variables, the mathematical formulation, the sensitivity analysis, and the filtering technique. Sec. 4 demonstrates the potential of using the additional families by studying several numerical examples and comparing the obtained results with those of just employing one family. Finally, a conclusion is presented in Sec. 5.

## 2 DESIGN OF THE TWO-SCALE STRUCTURE

In this section, we describe the technique we use in modeling cellular structures. We adopt the concept of two-scale structure and discretize the macro-structure into  $N$  micro-structures and then each micro-structure into  $M$  micro-elements. The superscripts MA and MI are used for referring to the macro-scale and micro-scale, respectively, and the design and evaluation methods are introduced in the following subsections.

### 2.1 Design of the Micro-structures

In mechanics, the equivalent compliance of two or more parallel Hookean springs is the reciprocal of the sum of reciprocals of the individual compliances, which is lower than the minimum one. As a novel strategy to achieve better mechanical properties, namely, effective elastic moduli, we mimic this feature by introducing a new micro-structure, denoted as XX-shaped, and constructed by stacking (connecting) two X-shaped structures horizontally. We then use three families of micro-structures to optimize structural problems. The first family is the conventional one that contains lattices obtained by superimposing parameterized X-shaped and square-shaped micro-structures, see Fig. 1c. The second family is generated by superimposing parameterized XX-shaped and square-shaped micro-structures. The third family contains the orthogonally rotated members of the second family. Fig. 2 shows selected micro-structures (members) from the introduced families. To the best knowledge of the authors, the second and third families have not yet been introduced in the literature. A lattice similar to the XX-shaped was used in the work of J. Hu et al. [14].

To include the three families in the optimization process, a two-parameter description is needed; one parameter indicates the selected family and the other one indicates the member inside the family. The two-parameter description is given in detail in Sec. 2.3.

## 2.2 Evaluation of the Effective Properties of Micro-structures

We treat the micro-structures as composite structures consisting of two isotropic materials, stiff and soft. The former material has Young's modulus of  $E_{\text{solid}} = 1$  and represents the solid micro-elements while the latter one has Young's modulus of  $E_{\text{void}} = 10^{-6}$  and represents the voids. To evaluate the effective elasticity tensor of the micro-structures, we use the homogenization theory which finds a homogenized elasticity tensor that reflects the mechanical behavior of complex materials with a periodic micro-structure by analyzing the repetitive unit [10, 11]. According to homogenization theory, the equivalent elasticity tensor of a periodic composite structure is obtained by

$$E_{ijkl}^H = \frac{1}{|\Omega|} \int_{\Omega} E_{pqrs} \left( \epsilon_{pq}^{0(ij)} - \epsilon_{pq}^{(ij)} \right) \left( \epsilon_{kl}^{0(rs)} - \epsilon_{kl}^{(rs)} \right) d\Omega, \quad (1)$$

where  $\Omega$  and  $|\Omega|$  are the domain and volume of the micro-structure, respectively;  $E_{pqrs}$  is the locally varying stiffness tensor;  $\epsilon_{pq}^{0(ij)}$  is the prescribed macroscopic strain field;  $\epsilon_{pq}^{(ij)}$  is the locally varying strain field; and  $i, j, k, l, p, q, r$  and  $s$  are the directions, i.e.  $\{1, 2, 3\}$  for 3D or  $\{1, 2\}$  for 2D.

The homogenization is performed numerically by discretizing the micro-structures into  $M$  micro-elements and solving the elasticity problem of Eq. (1) using the FEM. Then, the effective elastic tensor is obtained by

$$E_{ijkl}^H = \frac{1}{|\Omega|} \sum_{e=1}^M \left( \mathbf{u}_e^{(ij)} \right)^T \mathbf{k}_e \mathbf{u}_e^{(kl)}, \quad (2)$$

where  $\mathbf{k}_e$  is the stiffness matrix for the micro-element  $e$ ; and  $\mathbf{u}_e^{(ij)}$  is the element displacement solution corresponding to the unit strain field  $\epsilon^{0(ij)}$ . For a 2D space, as in our work, we need to consider only three macroscopic strain fields; namely unit strain in the first axis  $\epsilon_{pq}^{0(11)}$ , unit strain in the second axis  $\epsilon_{pq}^{0(22)}$ , and unit shear strain  $\epsilon_{pq}^{0(12)}$ . Then, Eq. (2) yields:

$$E_{ij}^H = \frac{1}{|\Omega|} \sum_{e=1}^M \left( \mathbf{u}_e^{(i)} \right)^T \mathbf{k}_e \mathbf{u}_e^{(j)},$$

and the effective elastic tensor is expanded as:

$$\mathbf{E}^H = \begin{bmatrix} E_{11}^H & E_{12}^H & E_{13}^H \\ E_{21}^H & E_{22}^H & E_{23}^H \\ E_{31}^H & E_{32}^H & E_{33}^H \end{bmatrix}. \quad (3)$$

In our study, we have generated new lattices by stacking several X-shaped sections horizontally and vertically, as shown in Fig. 3a. We use a unit cell of size  $1 \times 1$  consisting of  $114 \times 114$  bilinear plane-stress finite elements having Young's modulus and Poisson's ratio of 1 and 0.3, respectively, and a micro-scale volume fraction of  $V_f^{\text{MI}} = 50\% \pm 0.8$ . The equivalent mechanical properties of the generated lattices are obtained by following the procedure of Andreassen and Andreassen [2] and are plotted in Fig. 3b. As seen in Fig. 3b, stacking several X-shaped sections horizontally increases the effective elastic modulus in the horizontal axis,  $E_{11}^H$ , significantly, by 102%, 129%, 139%, 143%, and 146% for using two, three, four, five, and six sections, respectively. On the other hand, the effective elastic modulus in the vertical axis,  $E_{22}^H$ , decreases by 80%, 94%, 97%, 99%, and 99%, respectively, and the reductions in the two shear components,  $E_{33}^H$  and  $E_{12}^H$ , are (26%, 53%, 69%, 78%, and 84%) and (44%, 71%, 83%, 88%, and 92%). To have a good balance between the gain and reductions, we consider stacking only two X-shaped sections in the horizontal and vertical directions which leads us to the second and third families, respectively. Selected micro-structures from the three families are visualized in Fig. 2 and the effective elastic moduli of all micro-structures are plotted in Fig. 4.

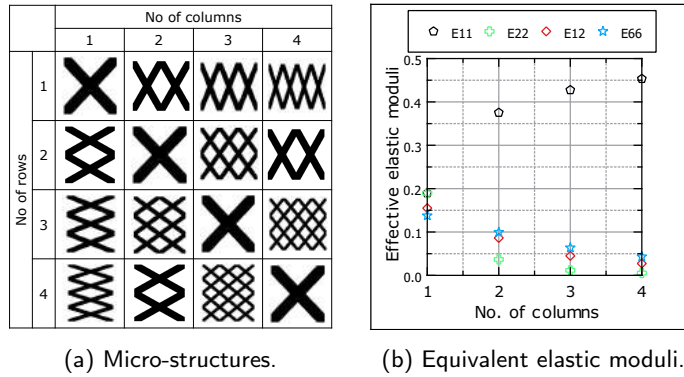


**Figure 3:** Stacked X-shaped micro-structures and their effective mechanical properties.

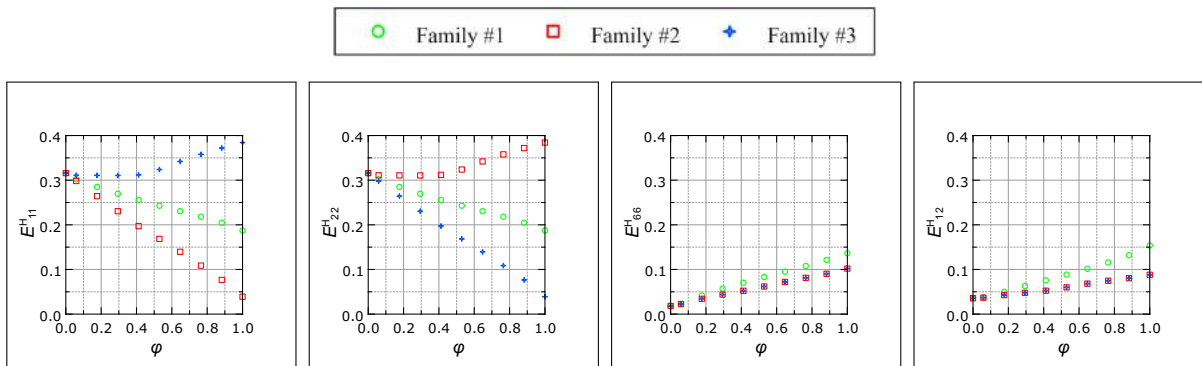


**Figure 4:** Effective elastic moduli for the micro-structures of the three families.

### 2.3 Finding the Relation Between the Micro-structures

After obtaining the constitutive matrices for the members of the three families, a relation between the members of the families is needed to facilitate the optimization process. For this purpose, a two-parameter description  $f(\psi, \varphi)$  is introduced, where  $\psi \in [0, 1]$  indicates the family, and  $\varphi \in [0, 1]$  indicates the member inside the family, i.e. the row and column, respectively, as illustrated in Fig. 2. The family is assigned according to

$$\text{Family} = \begin{cases} \text{Family \#2,} & 0 \leq \psi < \frac{1}{3} \\ \text{Family \#1,} & \frac{1}{3} \leq \psi < \frac{2}{3} \\ \text{Family \#3,} & \frac{2}{3} \leq \psi < 1 \end{cases} \quad (4)$$

and the corresponding member inside the selected family is assigned by rounding  $\varphi$  to the nearest lattice.

Then, the effective elastic moduli for all micro-structures, plotted in Fig. 4, are fitted in the least square sense using a bivariate polynomial of degree 3 in the direction of  $\varphi$  and of degree 2 in the direction of  $\psi$ . The gradients of these resulting polynomials are used in the sensitivity analysis in Sec. 3. It is worth noting that the order of the families, in Eq. (4), affects the optimization process and results. Accordingly, the families have been ordered in a manner that the interpolating surface has the lowest number of inflection points.

## 2.4 Design of the Macro-structure

The macro-structure is discretized into  $N$  macro-elements. Each macro-element, denoted as  $n$ , has three design variables that can have any value from 0 to 1. The first design variable is  $\rho_n$  and denotes the pseudo density while the second and third ones are  $\psi_n$  and  $\varphi_n$ , respectively, and indicate the family and family member, respectively, and their combination describes the geometry, as explained in the previous section.

$$\mathbf{E}_n(\rho_n, \psi_n, \varphi_n) = E_n^{\text{den}}(\rho_n) \mathbf{E}_n^{\text{geo}}(\psi_n, \varphi_n). \quad (5)$$

The first part  $E_n^{\text{den}}$  depends only on the density and is obtained by using modified Porous Anisotropic Material with Penalization (PAMP) [17], see Eq. (6). The second part  $\mathbf{E}_n^{\text{geo}}$  depends on the geometry and is computed through numerical homogenization, see Eq. (3)

$$E_n^{\text{den}} = E_{\min} + \rho_n^p (E_o - E_{\min}), \quad (6)$$

where  $p$  is a penalty factor to reduce the number of gray (intermediate) densities, typically  $p \geq 3$ ;  $E_o$  is Young's modulus of the material;  $E_{\min}$  is a very small number to prevent the singularity of the stiffness matrix, here we use  $E_{\min} = E_o \cdot 10^{-6}$ .

## 3 FORMULATION OF THE TOPOLOGY OPTIMIZATION PROBLEM

In this section, we describe the optimization problem by defining the design variables, formulating the mathematical model, and analyzing and filtering the sensitivities. After that, we present the solution method.

### 3.1 Design Variables

As already discussed in the previous section, our proposed algorithm accounts for three design variables, and each of them can take any value of the interval  $[0,1]$ . The design variables are  $\boldsymbol{\rho} = \{\rho_1, \rho_2, \rho_3, \dots, \rho_N\}^T$ ,  $\boldsymbol{\psi} = \{\psi_1, \psi_2, \psi_3, \dots, \psi_N\}^T$ , and  $\boldsymbol{\varphi} = \{\varphi_1, \varphi_2, \varphi_3, \dots, \varphi_N\}^T$  where  $N$  is the total number of macro-elements. These design variables are optimized in three steps to avoid unfavorable local minima. In the first step, only the first design parameter is optimized. Then, both the first and second design parameters are optimized simultaneously in the second step, and finally, in the third step, the first and third design parameters are optimized simultaneously.

### 3.2 Defining the Optimization Problem

The mathematical formulation of the optimization problem is as follows  
min.

$$C(\boldsymbol{\rho}, \boldsymbol{\psi}, \boldsymbol{\varphi}) = \mathbf{F}^T \mathbf{U}(\boldsymbol{\rho}, \boldsymbol{\psi}, \boldsymbol{\varphi}) = \mathbf{U}^T(\boldsymbol{\rho}, \boldsymbol{\psi}, \boldsymbol{\varphi}) \mathbf{K}(\boldsymbol{\rho}, \boldsymbol{\psi}, \boldsymbol{\varphi}) \mathbf{U}(\boldsymbol{\rho}, \boldsymbol{\psi}, \boldsymbol{\varphi}) \quad (7)$$

s.t.

$$\mathbf{K}(\boldsymbol{\rho}, \boldsymbol{\psi}, \boldsymbol{\varphi}) \mathbf{U}(\boldsymbol{\rho}, \boldsymbol{\psi}, \boldsymbol{\varphi}) = \mathbf{F}, \quad (8)$$

$$G(\boldsymbol{\rho}) = \sum_{n=1}^N \rho_n - N \cdot V_f^{\text{MA}} \leq 0,$$

and

$$0 \leq \rho_n \leq 1,$$

$$0 \leq \psi_n \leq 1,$$

$$0 \leq \varphi_n \leq 1,$$

where the objective function  $C$  is the structural compliance;  $\mathbf{K}$ ,  $\mathbf{U}$ , and  $\mathbf{F}$  are the global stiffness matrix, displacement vector, and force vector, respectively;  $G$  is an inequality constraint; and  $V_f^{MA}$  is the maximum allowed macro-scale volume fraction. The global stiffness matrix is obtained from the local stiffness matrices:

$$\mathbf{K}(\rho, \psi, \varphi) = \sum_{n=1}^N \mathbf{k}_n(\rho_n, \psi_n, \varphi_n)$$

with

$$\mathbf{k}_n(\rho_n, \psi_n, \varphi_n) = \int_{\Omega} \mathbf{B}^T \mathbf{E}_n(\rho_n, \psi_n, \varphi_n) \mathbf{B} \, d\Omega, \quad (9)$$

where  $\mathbf{k}_n$  is the stiffness matrix of element  $n$ ;  $\mathbf{B}$  is the strain-displacement matrix; and  $\mathbf{E}_n$  is the constitutive matrix for element  $n$  obtained by using Eq. (5).

### 3.3 Sensitivity Analysis

Here, we obtain the sensitivities using the direct approach. The objective function  $C$ , introduced in Eq. (7), can be written in a discretized form as:

$$C = \sum_{n=1}^N \mathbf{u}_n^T \mathbf{k}_n \mathbf{u}_n,$$

where  $\mathbf{u}_n$  is the nodal displacement vector of the macro-element  $n$ . The derivative of the objective function  $C$  with respect to  $\rho_n$  is given as:

$$\frac{\partial C}{\partial \rho_n} = \frac{\partial}{\partial \rho_n} \sum_{n=1}^N \mathbf{u}_n^T \mathbf{k}_n \mathbf{u}_n = \sum_{n=1}^N \frac{\partial \mathbf{u}_n^T}{\partial \rho_n} \mathbf{k}_n \mathbf{u}_n + \sum_{n=1}^N \mathbf{u}_n^T \frac{\partial \mathbf{k}_n}{\partial \rho_n} \mathbf{u}_n + \sum_{n=1}^N \mathbf{u}_n^T \mathbf{k}_n \frac{\partial \mathbf{u}_n}{\partial \rho_n}. \quad (10)$$

The derivative of the equilibrium constraint with respect to  $\rho_n$  is obtained from Eq. (8) by:

$$\mathbf{K} \frac{\partial \mathbf{U}}{\partial \rho_n} + \frac{\partial \mathbf{K}}{\partial \rho_n} \mathbf{U} = 0.$$

Similarly, we get:

$$\mathbf{k}_n \frac{\partial \mathbf{u}_n}{\partial \rho_n} = -\frac{\partial \mathbf{k}_n}{\partial \rho_n} \mathbf{u}_n. \quad (11)$$

By combining Eqs. (10) and (11), we get:

$$\frac{\partial C}{\partial \rho_n} = -\mathbf{u}_n^T \frac{\partial \mathbf{k}_n}{\partial \rho_n} \mathbf{u}_n. \quad (12)$$

Similarly, the derivatives of the objective function  $C$  with respect to  $\psi$  and  $\varphi$  are defined as:

$$\frac{\partial C}{\partial \psi_n} = -\mathbf{u}_n^T \frac{\partial \mathbf{k}_n}{\partial \psi_n} \mathbf{u}_n \quad (13)$$

and

$$\frac{\partial C}{\partial \varphi_n} = -\mathbf{u}_n^T \frac{\partial \mathbf{k}_n}{\partial \varphi_n} \mathbf{u}_n, \quad (14)$$

respectively. By applying Eq. (9) in Eqs. (12), (13), and (14), we get:

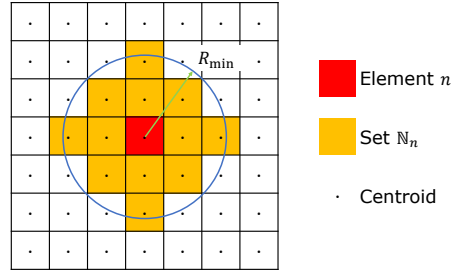


**Figure 5:** Filter size and neighboring elements.

$$\frac{\partial C}{\partial \rho_n} = -p\rho_n^{p-1} (E_o - E_{\min}) \mathbf{u}_n^T \left( \int_{\Omega_n} \mathbf{B}^T \mathbf{E}_n^{\text{geo}} \mathbf{B} d\Omega_n \right) \mathbf{u}_n,$$

$$\frac{\partial C}{\partial \psi_n} = -E_n^{\text{den}} \mathbf{u}_n^T \left( \int_{\Omega_n} \mathbf{B}^T \frac{\partial E_n^{\text{geo}}}{\partial \psi_n} \mathbf{B} d\Omega_n \right) \mathbf{u}_n,$$

and

$$\frac{\partial C}{\partial \varphi_n} = -E_n^{\text{den}} \mathbf{u}_n^T \left( \int_{\Omega_n} \mathbf{B}^T \frac{\partial E_n^{\text{geo}}}{\partial \varphi_n} \mathbf{B} d\Omega_n \right) \mathbf{u}_n,$$

where the terms  $\partial \mathbf{E}_n^{\text{geo}} / \partial \psi_n$  and  $\partial \mathbf{E}_n^{\text{geo}} / \partial \varphi_n$  are obtained from the gradients of the interpolating functions, as discussed in Sec. 2.3. Finally, the sensitivity of the second constraint, i.e.  $G$ , with respect to  $\rho_n$  is defined as:

$$\frac{\partial G(\rho)}{\partial \rho_n} = 1.$$

### 3.4 Filtering the Sensitivities and Design Variables

In order to prevent the checkerboard problem, we apply the sensitivity filter [22] to the derivatives of the first design variables, as

$$\frac{\partial \hat{C}}{\partial \rho_n} = \frac{\sum_{m \in \mathbb{N}_n} H_{nm} \rho_m \frac{\partial C}{\partial \rho_m}}{\max(\rho_n, \gamma) \sum_{m \in \mathbb{N}_n} H_{nm}},$$

where  $\partial \hat{C} / \partial \rho_n$  and  $\partial C / \partial \rho_n$  are the filtered and non-filtered sensitivities;  $\gamma = 10^{-3}$  is a small positive number to avoid singularity;  $H_{nm}$  is a weight factor given by

$$H_{nm} = R_{\min} - \text{dist}(n, m),$$

and  $\mathbb{N}_n$  is a set containing the neighboring elements of element  $n$  whose centers lie within a circle of a predefined radius  $R_{\min}$  called the filter size and given relative to the element size.  $\mathbb{N}_n$  is illustrated in Fig. 5 and given by

$$\mathbb{N}_n = \{m : \text{dist}(n, m) \leq R_{\min}\},$$

where  $\text{dist}(n, m)$  is the distance between the centers of element  $n$  and element  $m$ .

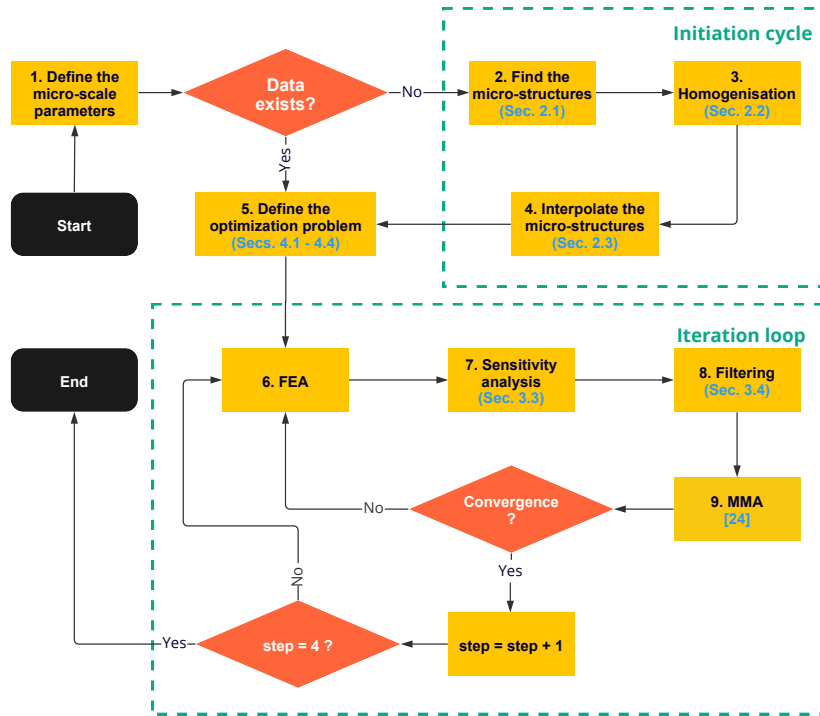


**Figure 6:** Flowchart of the algorithm.

Furthermore, to have a uniform transformation between the micro-structures, we apply the density filter [3] to the second and third design variables as

$$\frac{\partial \hat{C}}{\partial \xi_n} = \frac{\sum_{m \in \mathbb{N}_n} H_{nm} \frac{\partial C}{\partial \xi_m}}{\sum_{l \in \mathbb{N}_m} H_{ml}},$$

where  $\xi_n$  is either  $\psi_n$  or  $\varphi_n$ .

### 3.5 Solving the Optimization Problem

Fig. 6 summarizes the solution procedure of our proposed optimization algorithm. Firstly, we define the micro-structures' parameters (number of micro-elements and the micro-scale volume fraction). Then, the algorithm finds all the possible micro-structures having the given parameters, as discussed in Sec. 2.1. After that, we evaluate the effective elasticity matrices of the micro-structures and find their relations and gradients, as discussed in Secs. 2.2 and 2.3, respectively. Secondly, we define the optimization problem (i.e. initial design variables, dimensions of the design domain, number of macro-elements, macro-scale volume fraction, Young's modulus, Poisson's ratio, penalization factor, filter type, and minimum radius) and the algorithm starts the iteration loop by performing an FEA followed by a sensitivity analysis and filtering process as described in Secs. 3.3 and 3.4, respectively. Then, the design variables are updated in three steps using the Method of Moving Asymptotes (MMA) [23]. In the first step, we optimize only  $\rho$ , while in the second and third steps, we concurrently optimize  $\rho$  &  $\psi$ , and  $\rho$  &  $\varphi$ , respectively. In each step, we repeat the iteration loop until the relative improvement in the objective value is less than 0.1% for ten successive iterations. To avoid the

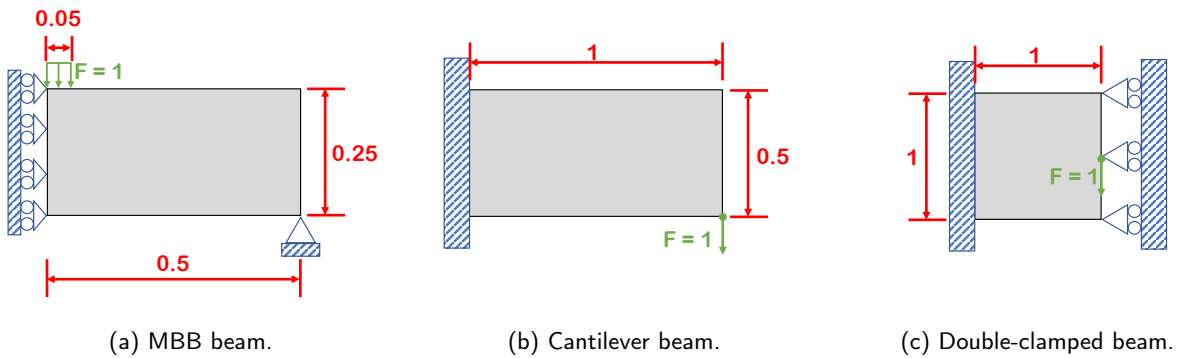


**Figure 7:** Models of the numerical problems.

extensive computation work needed for the numerical homogenization (process 3), we store the results of the initiation cycle (processes 2 – 4) and read them for the other optimization problems. We need to re-run the initiation cycle only if we change the micro-structures' parameters.

## 4 NUMERICAL EXAMPLES

To illustrate the capability of the proposed algorithm, several numerical problems, see Fig. 7, have been solved and will be presented in this section. The algorithm has been implemented in Spyder IDE 5.1.5 (Python 3.7.9 64-bit | Qt 5.12.10 | PyQt5 5.12.3) and all computations have been performed using an HP ZBook Firefly 15 G7 Mobile Workstation with two Intel® Core™ i7-10610U CPUs (1.80GHz and 2.30 GHz) equipped with a 32GB RAM and running Windows 10 Enterprise (64-bit) system. We use dimensionless quantities. The Young's modulus and the Poisson's ratio of the used material equal 1.0 and 0.3, respectively, and the initial values of  $\rho_n$ ,  $\psi_n$  and  $\varphi_n$  are selected as  $V_f^{MA}$ , 0.5 and 0.5, respectively. The minimum radii of the filters are chosen to be  $R_{min} = 2.0$ , i.e. two times the element length, and the penalty factor is set to  $p = 3$ , and the micro-scale structures are discretized into  $114 \times 114$  uniformly-sized plane-stress square elements and all the default values of the MMA are accepted. The CPU time for the Initiation Cycle, processes 2 – 4 in Fig. 6, is 144 seconds.

### 4.1 MBB Beam

As a first example, we consider a Messerschmitt-Bolkow-Blohm (MBB) beam problem. The beam has a length and height of 1.00 and 0.25, respectively, and holds a vertically distributed force having a magnitude of 1.00 and applied over the central 10% of its upper surface. Due to the symmetry, only the right half of the problem is considered and modeled using  $50 \times 25$  equally sized square elements, as shown in Fig. 7a. The macro-scale volume fraction was set to  $V_f^{MA} = 40\%$  and the problem is solved according to the methodology in Sec. 3.5 and Fig. 8a shows the iteration curves of the objective and the constraint. The iteration process converges after 88 cycles and the optimized design has compliance and a micro-scale volume fraction of 317.46 and 40.00%, respectively. In the first five cycles, compliance decreases steeply from 2865.79 down to 1017.90 (–64.5%), continues decreasing to 442.36 (–84.6%) at the end of the first step (Fig. 9b), then decreases gradually to 362.93 (–87.3%) at the end of the second step (Fig. 9d), and finally converges to 317.46 (–88.9%) at the end of the third step (Fig. 9f). The micro-scale volume fraction fluctuates during the first 20 iterations and stabilizes then. Fig. 9 shows the optimization process of the MBB beam problem. The optimized values of  $\rho$ ,  $\psi$ , and  $\varphi$  are plotted in the upper, middle, and lower subplots, respectively. Generally, the distribution of

the material is consistent with the directions of principal stress lines and the distribution of the micro-structures is homogenous except for some small regions. This may lead to some disconnected micro-structures but the used ones have fairly good connectivity at the corners without the need of setting some passive elements (non-designable region) which results in some compromises. Particularly, the horizontal structural parts mainly consist of brown micro-structures ( $\varphi_n \geq 0.65$ ) from family #3. As illustrated in Fig. 4, these micro-structures have the highest stiffness along the horizontal direction which is consonant with the direction of their principal strain. On the other hand, the oblique structural parts are mainly composed of dark brown micro-structures ( $\varphi_n \geq 0.9$ ) from family #1 which exhibit the highest shear stiffness. To evaluate our optimized design, we solve the same problem using only the conventional family of micro-structures, i.e. family #1. The optimized topologies of the MBB beam using the proposed and existing designs are shown in Fig. 10a and Fig. 10b, respectively. The conventional design converges to compliance of 340.68 which is 7.3% higher than our design.

## 4.2 Cantilever Beam

In the second example, we consider a cantilever beam problem. The beam has a length and height of 1.0 and 0.5, respectively, and holds a concentrated load of 1.0 at its lower left corner, see Fig. 7b. The problem is modeled by using  $160 \times 80$  equally sized square elements and the macro-scale volume fraction is set to 45%. The iteration process converges after 67 cycles and the optimized design has compliance and volume fraction of 275.38 and 44.96%, respectively, as shown in Fig. 8b and Fig. 11. Similar to the MBB beam, the upper and lower structural parts are filled with brown ( $\varphi_n \geq 0.6$ ) micro-structures from family #3 which give high stiffness along the horizontal direction. In between, we found darker micro-structures but belonging to family #1 ( $\varphi_n \geq 0.9$ ) because of their shear stiffness. Near the loading area, the highest stiffness along the vertical direction is achieved by the dark ( $\varphi_n \geq 0.7$ ) micro-structures from family #2.

## 4.3 Double Clamped Beam

The third example is a double-clamped beam problem. The beam has a length and height of 2.0 and 1.0, respectively, and holds a concentrated load with a magnitude of 1.0 at its middle, as shown in Fig. 7c. The left half of the problem is represented by  $50 \times 50$  equally sized square elements and symmetric boundary conditions are applied to the right edge. The micro-scale volume fraction is selected as 30% and the iteration process converges after 100 cycles and the optimized design has compliance and a volume fraction of 73.26 and 30.00%, respectively. The optimization history is plotted in Fig. 8c. As seen in Fig. 12, the optimized design is

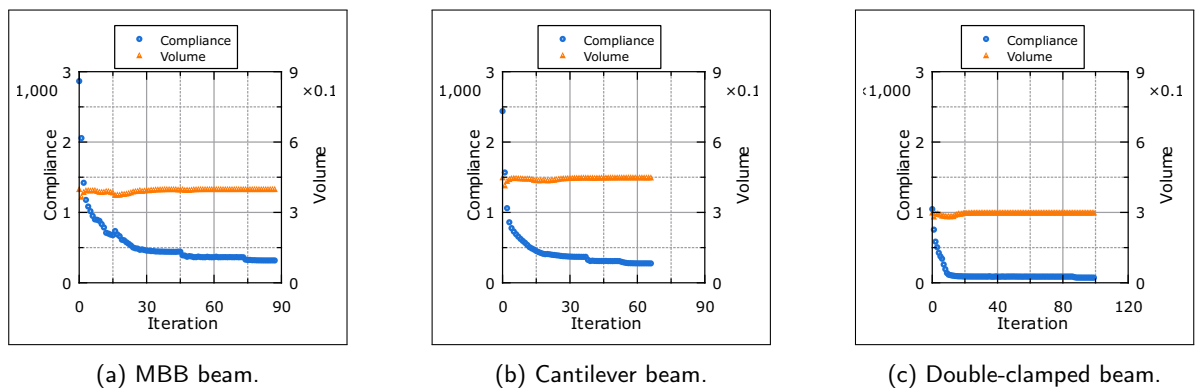


**Figure 8:** Optimization history of the objective (compliance) and constraint (volume).

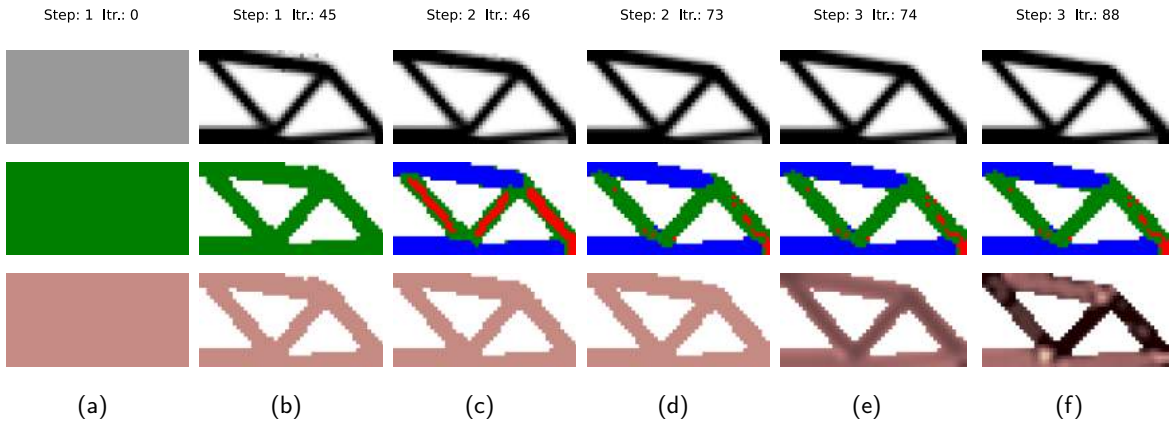


**Figure 9:** MBB beam: (a) initial design, (b-e) intermediate designs, and (f) optimized design.

symmetric along the horizontal axis and mainly composed of family #1 micro-structures with ultimate shear stiffness ( $\varphi_n \geq 0.8$ ) with some regions from family #3. Near the loading and symmetry boundary conditions, two clusters are seen; dark brown micro-structures from family #2 ( $\varphi_n \geq 0.8$ ) and beige micro-structures ( $\varphi_n \leq 0.1$ ). The former exhibits superior stiffness along the vertical direction while the latter possesses a good balance of stiffness along the horizontal and vertical directions which results in enhanced bending stiffness.

#### 4.4 Comparison of the Optimized Designs

To demonstrate the advantage of using our proposed method, we also solve the previous examples using the following methods: (1) employing only the conventional family #1 of micro-structures, i.e. fixing  $\psi_n = 1/2$ , (2) employing only the first new family #2, i.e. fixing  $\psi_n = 1/6$ , (3) employing only the second new family #3, i.e. fixing  $\psi_n = 5/6$ , and (4) employing the three families by optimizing the three design variables concurrently, i.e. in one step rather than three. The optimized designs from methods (1) - (3) are shown in Fig. 13 and their compliances (normalized to our method) are presented in Tab. 1. Obviously, our proposed method always gives better structural compliance. When comparing the results with the conventional family only and the here proposed combination of three families quantitatively, the biggest improvement is 7% in the cantilever beam problem, the least improvement is 0.9% in the double-clamped beam problem, and the

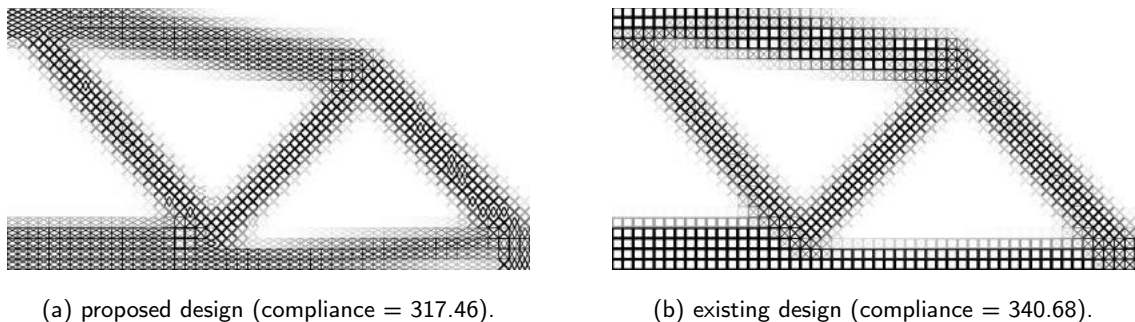


**Figure 10:** MBB beam: optimized topology using the proposed (a) and existing designs (b).

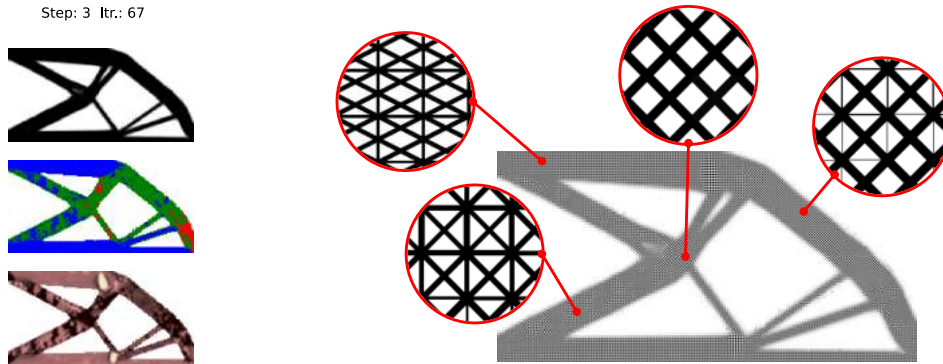


**Figure 11:** Cantilever beam: optimized design (left) and optimized topology (right).

improvement in the MBB is 6.2%. We conclude that employing only one family is not giving benefits such as using our proposed method which considers the three families together and results in optimized designs with lower structural compliances.

For method (4), the optimization process was found to be strongly dependent on the initial values of the second and third design variables. We attribute this effect to the number of used design variables. The higher the number of design variables, the more local minima arise making finding the best starting point more problematic. Similar problems are reported in [9, 28, 29]. However, we tested nine different starting points and compared their results with our proposed formulation. The optimized compliances are given in Tab. 2 and the optimized designs for the first example are shown in Fig. 14. A first look in Tab. 2 indicates that the concurrent formulation results in better results for both the cantilever beam and the double-clamped beam. But this is not true because of the random distributions of micro-structures (red, green, and blue colors in Fig. 14). These random distributions are observed all over the optimization process and violate the limitation of the assumed homogenization and thus may reflect artificial stiffening therefore a quantitative comparison is not possible and when we compare them qualitatively, i.e. Fig. 9f vs. Fig. 14, we find that the three steps formulation provide optimized designs having very less random distributions compared to the single step formulation.

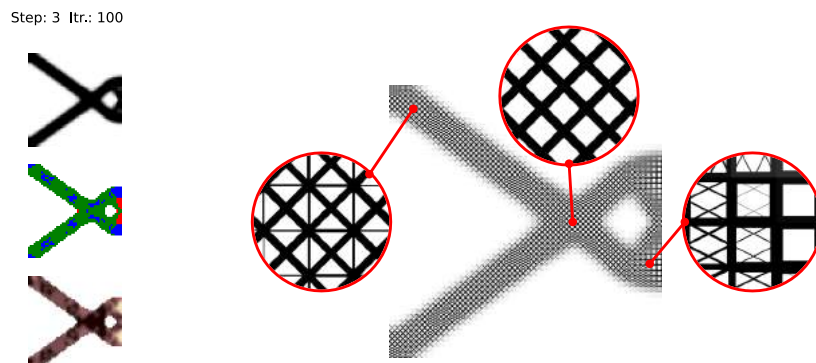


**Figure 12:** Double-clamped beam: optimized design (left) and optimized topology (right).

Employed family	Optimized compliance (normalized)		
	MBB beam	Cantilever beam	Double-clamped beam
#1	1.062	1.070	1.009
#2	1.119	1.035	1.040
#3	1.156	1.187	1.379

**Table 1:** Optimized compliance employing only one family.

## 5 CONCLUSION

The objective of this work was to enhance the optimization of functionally graded lattice structures. Firstly, we proposed two new families of micro-structures sharing similar geometric features and having higher effective elastic moduli in the horizontal and vertical axis. The first family was generated by superimposing parameterized XX-shaped and square-shaped micro-structures while the second one was generated by simply rotating the members of the first family by  $90^\circ$ . Secondly, we presented a two-scale topology optimization procedure that navigates between the three families of micro-structures; the proposed ones besides the existing family of superimposing two parameterized X-shaped and square-shaped micro-structures. The formulation consists of three design variables and the optimization is done in three steps. In each step, a distinct set of design variables is optimized. Thirdly, three numerical optimization problems for minimizing structural compliance were solved to illustrate the capability of the proposed procedure. The results showed that the optimized designs have not only better stiffnesses compared to the use of just the existing family of micro-structures but also have more uniform distributions of micro-structures. Based on this study, we conclude the following: (1) Adding the proposed micro-structural families to the existing ones is regarded as an efficient improvement in designing FGLs and results in a better stiffness-to-weight ratio, (2) Solving our three-design-variable problem in three steps results in lower initial guesses dependency and similar computational cost compared to the one-step approach, and (3) Due to its blurring effect, applying density filter to the second and third design variables gives smoother transitions between the micro-structures than the sensitivity filter. One of our next steps involves tests on 3D printing examples to experimentally validate the proposed model under the constraints of real additive manufacturing. Moreover, we will conduct further research in the future to improve the filtering process and expand the proposed families to include multi-material structures and transfer the method into the 3D domain.

	MBB beam			Cantilever beam			Double-clamped beam			
	$\varphi_o =$	0.0	0.5	1.0	0.0	0.5	1.0	0.0	0.5	1.0
	0.0	1.013	1.053	1.027	0.972	0.976	0.998	0.972	0.973	0.959
	$\psi_o =$ 0.5	1.034	1.036	1.013	0.967	0.985	0.972	0.962	0.968	0.971
	1.0	1.015	1.005	1.040	0.966	0.978	0.975	0.970	0.978	0.976

**Table 2:** Optimized compliance (MBB beam, normalized) employing the three families using the one-step formulation.

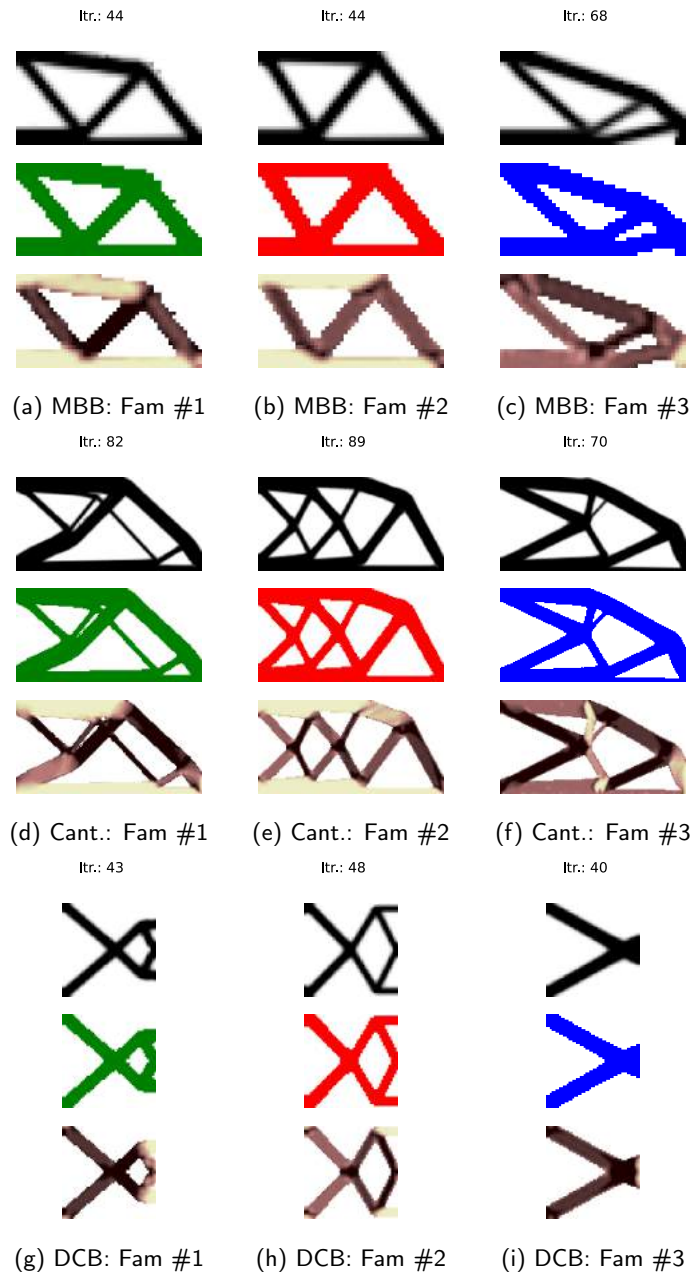


**Figure 13:** Optimized designs using different methods.

## ACKNOWLEDGEMENTS

The research presented in this paper has been supported by the Federal Ministry for Digital and Economic Affairs (BMDW) within the framework of COIN “Aufbau”, 8th call of the Austrian Research Promotion Agency (FFG) – project number 884136 (iLEAD).

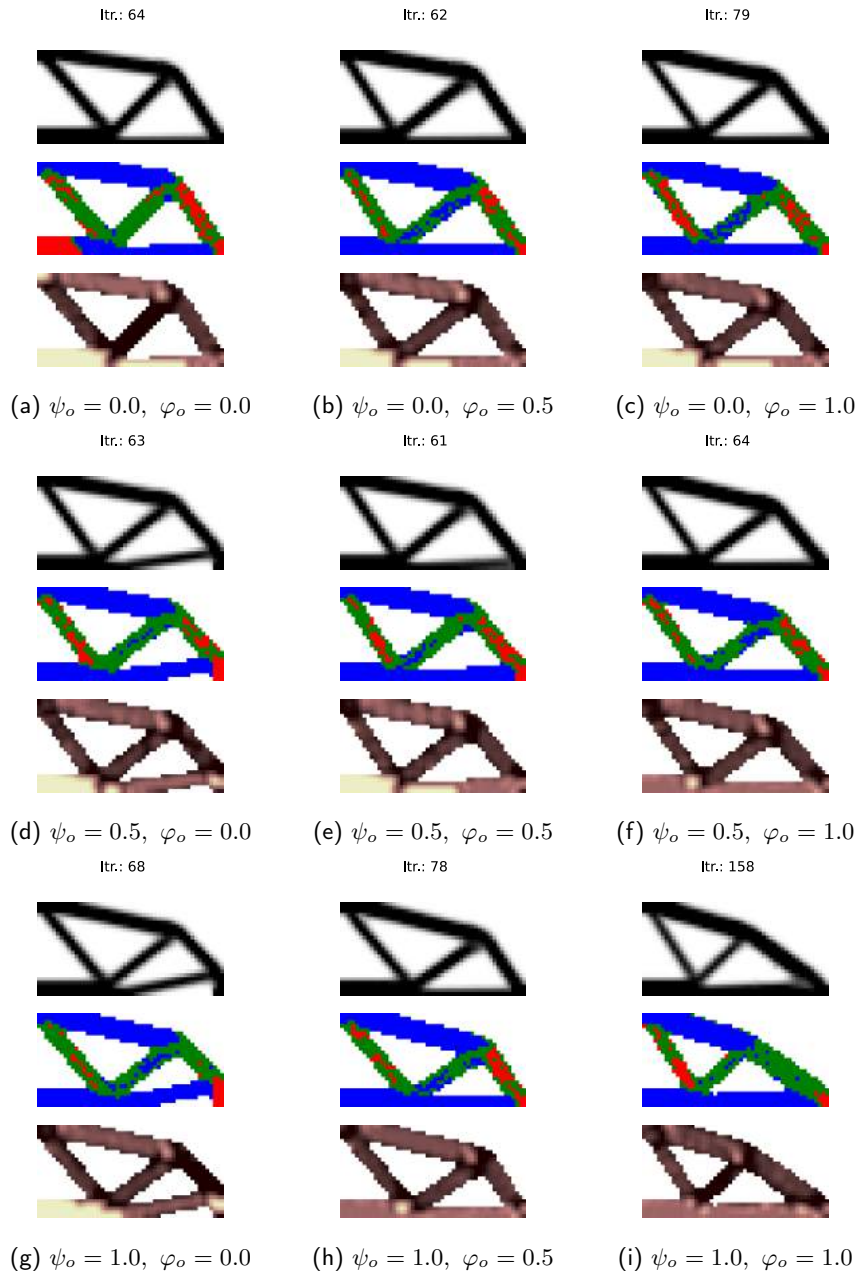


**Figure 14:** MBB beam: effect of the initial guess when using a single step formulation.

## ORCID

Ahmed Mohamed Jubartalla Ali, <http://orcid.org/0000-0001-7490-4545>

Lisa-Marie Faller, <http://orcid.org/0000-0001-8434-1440>

Margit Gföhler, <http://orcid.org/0000-0002-8977-8702>

Franz Riemelmoser, <http://orcid.org/0000-0003-1556-9059>

Mario Kapl, <http://orcid.org/0000-0001-8153-5987>

## REFERENCES

- [1] Al-Tamimi, A.A.; Almeida, H.; Bartolo, P.: Structural optimisation for medical implants through additive manufacturing. *Progress in Additive Manufacturing*, 5(2), 95–110, 2020. <http://doi.org/10.1007/s40964-020-00109-7>.
- [2] Andreassen, E.; Andreassen, C.S.: How to determine composite material properties using numerical homogenization. *Computational Materials Science*, 83, 488–495, 2014. <http://doi.org/10.1016/j.commatsci.2013.09.006>.
- [3] Bourdin, B.: Filters in topology optimization. *International journal for numerical methods in engineering*, 50(9), 2143–2158, 2001. <http://doi.org/10.1002/nme.116>.
- [4] Costa, M.R.; Sohoulı, A.; Suleman, A.: Multi-scale and multi-material topology optimization of gradient lattice structures using surrogate models. *Composite Structures*, 289, 2022. <http://doi.org/10.1016/j.compstruct.2022.115402>.
- [5] Da, D.; Cui, X.; Long, K.; Cai, Y.; Li, G.: Multiscale concurrent topology optimization of structures and microscopic multi-phase materials for thermal conductivity. *Engineering Computations*, 36(1), 126–146, 2019. <http://doi.org/10.1108/EC-01-2018-0007>.
- [6] Ding, H.; Xu, B.: A novel discrete–continuous material orientation optimization model for stiffness-based concurrent design of fiber composite. *Composite Structures*, 273, 114288, 2021. <http://doi.org/10.1016/j.compstruct.2021.114288>.
- [7] Fan, Z.; Yan, J.; Wallin, M.; Ristinmaa, M.; Niu, B.; Zhao, G.: Multiscale eigenfrequency optimization of multimaterial lattice structures based on the asymptotic homogenization method. *Structural and Multidisciplinary Optimization*, 61(3), 983–998, 2020. <http://doi.org/10.1007/s00158-019-02399-0>.
- [8] Gangwar, T.; Schillinger, D.: Concurrent material and structure optimization of multiphase hierarchical systems within a continuum micromechanics framework. *Structural and Multidisciplinary Optimization*, 63, 1175–1197, 2020. <http://doi.org/10.1007/s00158-021-02907-1>.
- [9] Gaynor, A.T.; Johnson, T.E.: Eliminating occluded voids in additive manufacturing design via a projection-based topology optimization scheme. *Additive Manufacturing*, 33, 101149, 2020. <http://doi.org/10.1016/j.addma.2020.101149>.
- [10] Hassani, B.; Hinton, E.: A review of homogenization and topology optimization ii—analytical and numerical solution of homogenization equations. *Computers & Structures*, 69(6), 719–738, 1998. [http://doi.org/10.1016/S0045-7949\(98\)00132-1](http://doi.org/10.1016/S0045-7949(98)00132-1).
- [11] Hassani, B.; Hinton, E.: A review of homogenization and topology optimization i - homogenization theory for media with periodic structure. *Computers and Structures*, 69(6), 707–717, 1998. [http://doi.org/10.1016/S0045-7949\(98\)00131-X](http://doi.org/10.1016/S0045-7949(98)00131-X).
- [12] Hoang, V.N.; Nguyen, N.L.; Tran, P.; Qian, M.; Nguyen-Xuan, H.: Adaptive concurrent topology optimization of cellular composites for additive manufacturing. *JOM*, 72(6), 2378–2390, 2020. <http://doi.org/10.1007/s11837-020-04158-9>.
- [13] Hoang, V.N.; Tran, P.; Nguyen, N.L.; Hackl, K.; Nguyen-Xuan, H.: Adaptive concurrent topology optimization of coated structures with nonperiodic infill for additive manufacturing. *CAD Computer Aided Design*, 129, 102918, 2020. <http://doi.org/10.1016/j.cad.2020.102918>.
- [14] Hu, J.; Luo, Y.; Liu, S.: Two-scale concurrent topology optimization method of hierarchical structures with self-connected multiple lattice-material domains. *Composite Structures*, 272, 2021. <http://doi.org/10.1016/J.COMPSTRUCT.2021.114224>.

- [15] Kim, J.E.; Park, K.: Multiscale topology optimization combining density-based optimization and lattice enhancement for additive manufacturing. *International Journal of Precision Engineering and Manufacturing - Green Technology*, 8(4), 1197–1208, 2021. <http://doi.org/10.1007/s40684-020-00289-1>.
- [16] Li, H.; Luo, Z.; Gao, L.; Qin, Q.: Topology optimization for concurrent design of structures with multi-patch microstructures by level sets. *Computer Methods in Applied Mechanics and Engineering*, 331, 536–561, 2018. <http://doi.org/10.1016/j.cma.2017.11.033>.
- [17] Liu, L.; Yan, J.; Cheng, G.: Optimum structure with homogeneous optimum truss-like material. *Computers and Structures*, 86(13-14), 1417–1425, 2008. <http://doi.org/10.1016/j.compstruc.2007.04.030>.
- [18] Liu, P.; Kang, Z.; Luo, Y.: Two-scale concurrent topology optimization of lattice structures with connectable microstructures. *Addit Manuf*, 36, 2020. <http://doi.org/10.1016/j.addma.2020.101427>.
- [19] Meng, L.; Zhang, W.; Quan, D.; Shi, G.; Tang, L.; Hou, Y.; Breitkopf, P.; Zhu, J.; Gao, T.: From topology optimization design to additive manufacturing: Today's success and tomorrow's roadmap. *Archives of Computational Methods in Engineering*, 27(3), 805–830, 2020. <http://doi.org/10.1007/s11831-019-09331-1>.
- [20] Michell, A.G.M.: LVIII. The limits of economy of material in frame-structures. *The London, Edinburgh, and Dublin Philosophical Magazine and Journal of Science*, 8(47), 589–597, 1904. <http://doi.org/10.1080/14786440409463229>.
- [21] Moreira, J.B.D.; de Souza Lisboa, E.; Rodrigues, G.C.; Link, F.B.; Casas, W.J.P.: Multiscale topology optimization for frequency domain response with bi-material interpolation schemes. *Optimization and Engineering*, 22, 2707–2739, 2021. <http://doi.org/10.1007/s11081-020-09550-7>.
- [22] Sigmund, O.: On the design of compliant mechanisms using topology optimization. *Mechanics of Structures and Machines*, 25(4), 493–524, 1997. <http://doi.org/10.1080/08905459708945415>.
- [23] Svanberg, K.: The method of moving asymptotes—a new method for structural optimization. *International journal for numerical methods in engineering*, 24(2), 359–373, 1987. <http://doi.org/10.1002/nme.1620240207>.
- [24] Wang, C.; Gu, X.; Zhu, J.; Zhou, H.; Li, S.; Zhang, W.: Concurrent design of hierarchical structures with three-dimensional parameterized lattice microstructures for additive manufacturing. *Structural and Multidisciplinary Optimization*, 61(3), 869–894, 2020. <http://doi.org/10.1007/s00158-019-02408-2>.
- [25] Wang, C.; Zhu, J.H.; Zhang, W.H.; Li, S.Y.; Kong, J.: Concurrent topology optimization design of structures and non-uniform parameterized lattice microstructures. *Structural and Multidisciplinary Optimization*, 58(1), 35–50, 2018. <http://doi.org/10.1007/s00158-018-2009-0>.
- [26] Wang, Y.; Hu, D.; Wang, H.; Zhang, T.; Yan, H.: Practical design optimization of cellular structures for additive manufacturing. *Engineering Optimization*, 52(11), 1887–1902, 2020. <http://doi.org/10.1080/0305215X.2019.1696785>.
- [27] Wei, N.; Ye, H.; Zhang, X.; Li, J.; Sui, Y.: Topology optimization for design of hybrid lattice structures with multiple microstructure configurations. *Acta Mechanica Solida Sinica*, 2022. <http://doi.org/10.1007/s10338-021-00302-3>.
- [28] Xia, L.; Breitkopf, P.: Design of materials using topology optimization and energy-based homogenization approach in matlab. *Structural and Multidisciplinary Optimization*, 52(6), 1229–1241, 2015. <http://doi.org/10.1007/s00158-015-1294-0>.
- [29] Xia, L.; Breitkopf, P.: Multiscale structural topology optimization with an approximate constitutive model for local material microstructure. *Computer Methods in Applied Mechanics and Engineering*, 286, 147–167, 2015. <http://doi.org/10.1016/J.CMA.2014.12.018>.

- [30] Yan, J.; Sui, Q.; Fan, Z.; Duan, Z.; Yu, T.: Clustering-based multiscale topology optimization of thermo-elastic lattice structures. *Computational Mechanics*, 66(4), 979–1002, 2020. <http://doi.org/10.1007/s00466-020-01892-4>.
- [31] Yu, H.; Hong, H.; Cao, S.; Ahmad, R.: Topology optimization for multipatch fused deposition modeling 3d printing. *Applied Sciences (Switzerland)*, 10, 3, 2020. <http://doi.org/10.3390/app10030943>.
- [32] Zhang, C.; Xu, S.; Liu, J.; Ma, Y.: Comprehensive clustering-based topology optimization for connectable multi-scale additive manufacturing structures. *Additive Manufacturing*, 54, 102786, 2022. <http://doi.org/10.1016/j.addma.2022.102786>.
- [33] Zhang, H.; Wang, Y.; Kang, Z.: Topology optimization for concurrent design of layer-wise graded lattice materials and structures. *International Journal of Engineering Science*, 138, 26–49, 2019. <http://doi.org/10.1016/j.ijengsci.2019.01.006>.
- [34] Zhou, H.; Zhu, J.; Wang, C.; Zhang, Y.; Wang, J.; Zhang, W.: Hierarchical structure optimization with parameterized lattice and multiscale finite element method. *Structural and Multidisciplinary Optimization*, 65(1), 1–20, 2022. <http://doi.org/10.1007/s00158-021-03149-x>.
- [35] Zhu, J.; Zhou, H.; Wang, C.; Zhou, L.; Yuan, S.; Zhang, W.: A review of topology optimization for additive manufacturing: Status and challenges. *Chinese Journal of Aeronautics*, 01(17), 2021. <http://doi.org/10.1016/j.cja.2020.09.020>.